DALTON
FULL PAPER

Synthesis, crystal structures and magnetic properties of linear and bent trinuclear complexes formed by hexacyanometallates and copper(II) complexes

Richard J. Parker,[a] Kevin D. Lu,[a] Stuart R. Batten,[a] Boujemaa Moubaraki,[a] Keith S. Murray,*[a] Leone Spiccia,*[a] John D. Cashion,[b] A. David Rae[c] and Anthony C. Willis[c]

[a] *School of Chemistry, Monash University, PO Box 23, Victoria, 3800, Australia. E-mail: leone.spiccia@sci.monash.edu.au*
[b] *School of Physics and Materials Engineering, Monash University, PO Box 27, Victoria, 3800, Australia*
[c] *Research School of Chemistry, Australian National University, Canberra, ACT 0200, Australia*

Received 13th June 2002, Accepted 29th July 2002
First published as an Advance Article on the web 10th September 2002

The bimetallic trinuclear complexes, $[\{(tpa)Cu(NC)\}_2Fe(CN)_4]ClO_4\cdot 6H_2O$ (**1**), $[\{(tren)Cu(NC)\}_2Fe(CN)_4]ClO_4\cdot 4H_2O$ (**2**), $[\{Cu(tpa)NC\}_2Cr(CN)_4]ClO_4\cdot 8H_2O$ (**3**) and $[\{Cu([15]aneN_4)NC\}_2Cr(CN)_4]ClO_4\cdot 4H_2O$ (**4**) [tpa = tris(2-pyridylmethyl)amine, tren = tris(2-aminoethyl)amine, ([15]aneN$_4$ = 1,5,9,12-tetraazacyclopentadecane] were prepared by addition of solutions of the Cu^{II} tpa, tren and [15]aneN$_4$ complexes to solutions of hexacyanometallate, $[M(CN)_6]^{3-}$ (M = Fe or Cr), in a 2:1 molar ratio. For **1**, an oxidant was added to prevent reduction of the Fe^{III} centre, while for **2**, the synthesis was carried out in acetonitrile. **1** Consists of quasi-linear trinuclear units of two *trans*-oriented $[Cu(tpa)]^{2+}$ ions linked to the central Fe^{III} core *via* two bridging cyano groups with the Cu^{II} centres residing in a distorted trigonal bipyramidal geometry. Use of a bis(bidentate) Cu(II) chelate, $[Cu(H_2LN_4)_2](NO_3)_2$ (H_2LN_4 = 1,1′,4,4′,5,5′,6,6′-octahydro-2,2′-bipyrimidine), yielded the first example of a non-linear *cis*-oriented trinuclear complex, $[\{(H_2LN_4)_2Cu(NC)\}_2Fe(CN)_4]NO_3\cdot 3H_2O$ (**5**), in which the Cu^{II} centres have a square pyramidal geometry. Magnetic studies on complex **1** show a rapid increase in the magnetic moment below 25 K, consistent with the presence of ferromagnetic coupling between the Fe^{III} (LS, $S = \frac{1}{2}$) and Cu^{II} ($S = \frac{1}{2}$) metal centres, where $g_{Cu} = g_{Fe} = 2.16$, $J_{12} = 4.3$ cm^{-1}, $J_{13} = -0.18$ cm^{-1}. The *cis*-complex, **5**, showed close to Curie-like behaviour and gave a good fit to the trimer model using $g_{Cu} = g_{Fe} = 2.31$, $J_{12} = 1.95$ cm^{-1}, $J_{13} = -2.1$ cm^{-1}. The Cu^{II}Cr^{III}Cu^{II} complex **4** also displayed ferromagnetic coupling across the Cr–CN–Cu bridges because of orthogonal t_{2g}(Cr)/e_g(Cu) orbital overlap. Best-fit parameters are $g = 2.1$, $J_{CuCr} = 1.31$ cm^{-1}, $J_{CuCu} = 0$ cm^{-1}. Complexes **2** and **3** showed related ferromagnetic behaviour but which fitted poorly to the trimer model.

Introduction

In recent years, recognition of the ability of the cyano group to bridge two metal centres and to promote ferromagnetic interactions has led to the application of hexacyanometallates as building blocks for bimetallic assemblies with 1-D chain, 2-D sheet and 3-D lattice structures and showing novel magnetic properties.[1–15] In addition to these polymers, hexacyanometallates have been used as templates for discrete bimetallic clusters.[16–31] Verdaguer and co-workers have reported detailed studies of two heptanuclear clusters, $[Cr\{(CN)Ni(L)\}_6](ClO_4)_9$ (L = tetraethylenepentamine) and $[Cr\{(CN)Mn(L)\}_6](ClO_4)_9$ [L = N,N,N′-tris(2-pyridylmethyl)-N′-methylethane-1,2-diamine],[20,21,26] in which $[Cr(CN)_6]^{3-}$ is encapsulated by either six Ni^{II} (S = 1) or six Mn^{II} (S = 5/2) moieties. We have reported the structures of several heptanuclear $[M_a\{(CN)M_bL\}_6]^{8+/9+}$ clusters, where M$_a$ = Fe^{II}, M$_b$ = Cu^{II} and L = tris(2-pyridylmethyl)amine (tpa);[22] M$_a$ = Fe^{II}, M$_b$ = Cu^{II} and L = tris(2-aminoethyl)amine (tren);[30] M$_a$ = Fe^{II}, M$_b$ = Mn^{II} and L = 1,4-bis(2-pyridylmethyl)-1,4,7-triazacyclononane (dmptacn);[31] M$_a$ = Cr^{III}, M$_b$ = Mn^{II} and L = dmptacn.[29] For the M$_a$ = Fe^{II}, M$_b$ = Cu^{II} and L = tren combination, a product has been isolated in which the heptanuclear $[M_a\{(CN)M_bL\}_6]^{8+}$ cluster and a pentanuclear $[(CN)_2M_a\{(CN)M_bL\}_4]^{5+}$ cluster have co-crystallised.[30] The formation of these products has been aided by the judicious choice of multidentate ligands (*i.e.* branched tetradentate ligands with Cu^{II} and pentadentate ligands with either Mn^{II} or Ni^{II}). The isolation of an octanuclear cluster, $[M_4Co_4(CN)_{12}(L^6)_8]^{12+}$,[24] with a cubic arrangement of metal ions, prepared from $[(tacn)M(OH_2)_3]^{3+}$ (M = Cr or Co) and $[(tacn)Co(CN)_3]$, and $[\{bpm)_2Ni\}_3\{Fe(CN)_6\}_2]$,[23] a neutral pentanuclear cluster prepared from $[(bpm)_2Ni(OH_2)_2]^{2+}$ and $[Fe(CN)_6]^{3-}$ [tacn = 1,4,7-triazacyclononane, bpm = bis(pyrazolyl)methane], further highlights the importance of the choice of co-ligand. It should be noted, however, that Hashimoto *et al.*[27] and Decurtins *et al.*[28] have been able to isolate discrete bimetallic clusters with very high spin ground states which do not have multidentate co-ligands (*viz.* the two isostructural $[Mn^{II}_9M_6^{V}]$ cyano-bridged clusters with M = W or Mo).

Efforts to elucidate structural features of M$_a$–C≡N–M$_b$-bridged clusters have led to the study of a few trinuclear complexes, *e.g.* $[\{(tren)Cu(NC)\}_2Fe^{II}(CN)_4]\cdot 12H_2O$.[25] The relevance of bridged binuclear iron–copper complexes to the enzyme cytochrome C oxidase has led a number of groups to develop discrete heteropolynuclear complexes incorporating iron porphyrin units.[16–19]

The paucity of bimetallic trinuclear complexes incorporating hexacyanometallates prompted us to prepare such complexes by reacting $[M^{III}(CN)_6]^{3-}$ (M = Fe, Cr) with the Cu^{II} complexes of polydentate ligands. The ligands exert some control on the nuclearity of the bimetallic product by occupying all but one

DOI: 10.1039/b205749m

coordination site on penta-coordinate Cu^{II} centres. We report here the synthesis and characterisation of five hetero-trinuclear complexes: $[\{(tpa)Cu(NC)\}_2Fe(CN)_4]ClO_4\cdot 6H_2O$ (**1**), $[\{(tren)Cu(NC)\}_2Fe(CN)_4]ClO_4\cdot 4H_2O$ (**2**), $[\{Cu(tpa)NC\}_2Cr(CN)_4]ClO_4\cdot 8H_2O$ (**3**) and $[\{Cu([15]aneN_4)NC\}_2Cr(CN)_4]ClO_4\cdot 4H_2O$ (**4**) ([15]aneN$_4$ = 1,5,9,12-tetraazacyclopentadecane), $[\{(H_2LN_4)_2Cu(NC)\}_2Fe(CN)_4]NO_3\cdot 3H_2O$ (**5**), (H_2LN_4 = 1,1′,4,4′,5,5′,6,6′-octahydro-2,2′-bipyrimidine). The complex cations are depicted in Fig. 1. Since completion of this work, another linear trinuclear Cu^{II}–Fe^{III}–Cu^{II} complex of a tetradentate Schiff-base ligand has been reported.[32]

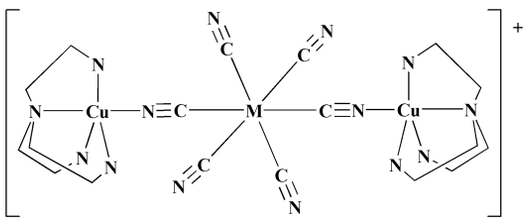

(**1**) M = Fe, L = tpa; (**2**) M = Fe, L = tren; (**3**) M = Cr, L = tpa

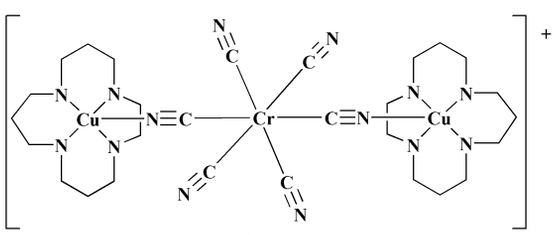

(**4**)

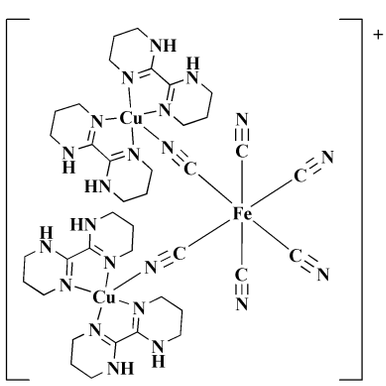

(**5**)

Fig. 1 Structures of the bimetallic trinuclear cations of complexes **1**–**5**.

Experimental

Physical measurements

Infrared spectra were recorded as KBr disks on a Bruker 1600 FTIR spectrometer and UV-visible spectra on a Cary 5G spectrophotometer. Electron microprobe analyses were made with a Jeol JSM-1 scanning electron microscope through an NEC X-ray detector and pulse processing system connected to a Packard multichannel analyser. Solid samples were mounted on an aluminium planchette and covered with a thin film of carbon using a Balzer Union CED 010 carbon sputterer. Variable temperature magnetic susceptibilities of homogeneous powders or polycrystalline samples were measured as described previously,[23] on a Quantum Design MPMS SQUID magnetometer (temp. range 4.2–300 K). Samples were contained in gelatin capsules which were held in the centre of a soda straw fused to the end of the sample rod. Mössbauer spectra were obtained in the transmission mode using a ^{57}Co in Rh source. The samples were crushed and placed in an iron-free polymer sample holder and the spectra recorded in the absence of an applied magnetic field. The isomer shifts were calibrated against natural α-iron foil at room temperature. Curve fitting was performed using least-squares procedures and employed Lorenztian line shapes.

Materials

Tris(2-pyridylmethyl)amine (tpa),[33] 1,1′,4,4′,5,5′,6,6′-octahydro-2,2′-bipyrimidine (H_2LN_4),[34] $[Et_4N]_3[Fe(CN)_6]$[35] and $K_3[Cr(CN)_6]$[36] were prepared by published procedures. All other chemicals and solvents were of reagent grade and were used without further purification.

CAUTION: Although no problems were encountered in this work, transition metal perchlorates are potentially explosive and should be prepared in small quantities. Due care must be taken when handling perchlorate and cyanide salts.

Syntheses

$[\{(tpa)Cu(NC)\}_2Fe(CN)_4]ClO_4\cdot 6H_2O$ (1). A solution of $Cu(ClO_4)_2\cdot 6H_2O$ (0.64 g, 1.72 mmol) in water (30 ml) was added to a stirred solution of tpa (0.50 g, 1.72 mmol) in water (30 ml), and the resulting royal blue solution stirred for a further 10 min. To this solution of $[Cu(tpa)OH_2](ClO_4)_2$, a solution of $K_3[Fe(CN)_6]$ (0.28 g, 0.86 mmol) containing an excess of $K_2S_2O_8$ (0.26 g, 0.95 mmol) in water (55 ml) was added dropwise, resulting in the immediate precipitation of **1** as a green powder. The product was collected by filtration, washed with water, ethanol and ether, and then air-dried (0.93 g, 95%). Green crystals suitable for X-ray diffraction studies were obtained by recrystallisation from a water–acetonitrile mixture (1:4 v/v). Analyses calc. for $C_{42}H_{48}N_{14}O_{10}ClCu_2Fe$: C 44.8; H 4.3; N 17.4; found: C 45.0; H 4.6; N 18.0%. Selected IR bands (cm^{-1}): ν(OH) 3419; ν[C≡N(b)] 2158; ν[C≡N(t)] 2122; ν(py) 1609, 1574m, 1482s, 1442s, 774vs; $\nu(ClO_4)$ 1114, 1090, 628. Electron microprobe: Cu, Fe, Cl present. UV-visible [λ_{max}/nm (ε_{max}/M^{-1}cm^{-1}); CH_3CN]: 423 (1220), 834 (446). Magnetic moment: μ_{eff} (295 K) = 3.35 μ_B per molecule.

$[\{Cu(tren)NC\}_2Fe(CN)_4]ClO_4\cdot 2H_2O$ (2). A solution of $[Cu(tren)(OH_2)][ClO_4]_2$ was prepared by adding a solution of $Cu(ClO_4)_2\cdot 6H_2O$ (0.370 g, 1.00 mmol) in CH_3CN (10 ml) to a stirred solution of tren (0.146 g, 1.00 mmol) in CH_3CN (10 ml). Dropwise addition of a solution of $[Et_4N]_3[Fe(CN)_6]$ (0.300 g, 0.50 mmol) in CH_3CN (15 ml) to the $[Cu(tren)(OH_2)][ClO_4]_2$ solution precipitated a bright green powder of $[\{Cu(tren)CN\}_2Fe(CN)_4]ClO_4\cdot 2H_2O$. The powder was collected by filtration and air-dried (0.316 g, 41%). Analyses calc. for $C_{18}H_{40}N_{14}O_6ClCu_2Fe$: C 28.2; H 5.3; N 25.6; found: C 28.2; H 5.2; N 25.4%. Selected IR bands (cm^{-1}): ν(OH) 3446vs br; ν(NH) 3325vs, 3267vs; ν[C≡N(b)] 2146s; ν[C≡N(t)] 2116vs; $\nu(ClO_4)$ 1115vs, 1089vs, 628s. Electron microprobe: Cu, Fe, Cl present. UV-visible [λ_{max}/nm (ε_{max}/M^{-1} cm^{-1}); DMSO]: 426 (1130), 665sh (224), 811 (298). Magnetic moment: μ_{eff} (290 K) = 3.56 μ_B per molecule.

$[\{Cu(tpa)NC\}_2Cr(CN)_4]ClO_4\cdot 8H_2O$ (3). A solution of $[Cu(tpa)(OH_2)][ClO_4]_2$ was prepared by adding $Cu(ClO_4)_2\cdot 6H_2O$ (0.376 g, 1.01 mmol) in water (50 ml) to a stirred solution of tpa (0.295 g, 1.02 mmol) in water (30 ml). A solution of $K_3[Cr(CN)_6]$ (0.166 g, 0.51 mmol) in water (25 ml) was then added dropwise, resulting in the immediate precipitation of a green–blue powder of **3**. This powder was filtered and washed with water and air-dried (0.417 g, 81%). Analyses calc. for $C_{42}H_{52}N_{14}O_{12}ClCu_2Cr$: C 43.5; H 4.5; N 16.9; found: C 43.6; H 3.9; N 16.7%. Selected IR bands (cm^{-1}): ν(OH) 3418vs br; ν[C≡N(b)] 2178s; ν[C≡N(t)] 2129m; ν(py) 1610vs, 1575m, 1482s, 1442vs, 774vs; $\nu[ClO_4]$ 1092vs, 628s. Electron microprobe: Cu, Cr, Cl present. UV-visible [λ_{max}/nm (ε_{max}/M^{-1} cm^{-1}); DMSO]: 598sh (215), 790 (471). Magnetic moment: μ_{eff} (295 K) = 4.74 μ_B per molecule.

[{Cu([15]aneN$_4$)NC}$_2$Cr(CN)$_4$]ClO$_4$·4H$_2$O (4). An aqueous solution of [Cu([15]aneN$_4$)(OH$_2$)][ClO$_4$]$_2$ was prepared *in situ* by addition of a solution of [15]aneN$_4$ (0.215 g, 1.00 mmol) in water (15 ml) to a stirred aqueous solution of Cu(ClO$_4$)$_2$·6H$_2$O (0.371 g, 1.00 mmol). A solution of K$_3$[Cr(CN)$_6$] (0.327 g, 1.00 mmol) in water (20 ml) was then added dropwise, resulting in a colour change from purple–blue to deep blue. Excess NaClO$_4$ (1.0 g) was added and the solution allowed to evaporate slowly at room temperature in the dark. Blue plates of **4** precipitated and were collected by filtration, washed with water and air-dried (0.31 g, 67%). Analyses calc. for C$_{28}$H$_{60}$N$_{14}$ClO$_8$Cu$_2$Cr: C 36.0; H 6.5; N 21.0; found: C 35.9; H 6.8; N 21.3%. Selected IR bands (cm^{-1}): ν(OH) 3386vs; ν(NH) 3234vs; ν[C≡N(t)] 2127s; ν(ClO$_4$) 1102m, 1066s, 628m. Electron microprobe: Cu, Cr, Cl present. UV-visible [λ_{max}/nm (ε_{max}/M^{-1} cm^{-1}); H$_2$O]: 375sh (168), 592 (333). Magnetic moment: μ_{eff} (294 K) = 4.85 μ_B per molecule.

[{(H$_2$LN$_4$)$_2$Cu(NC)}$_2$Fe(CN)$_4$]NO$_3$·3H$_2$O (5). K$_3$[Fe(CN)$_6$] (0.164 g, 0.5 mmol) and K$_2$S$_2$O$_8$ (0.2 g, 0.74 mmol) were dissolved in 15 ml of water to give a yellow solution. Separately, Cu(NO$_3$)$_2$·3H$_2$O (0.128 g, 0.53 mmol) and H$_2$LN$_4$ (0.160 g, 1.0 mmol) were dissolved in 25 ml of water to give a blue solution. Mixing of the two solutions gave a green precipitate of **5**, which was collected by filtration. Evaporation of the mother liquor yielded well-formed green crystals of **5** (0.60 g, 82%). Analyses calc. for C$_{38}$H$_{62}$N$_{23}$O$_6$Cu$_2$Fe: C 40.7; H 5.6; N 28.8; found: C 40.2; H 5.4; N 27.4%. Selected IR bands (cm^{-1}): ν[OH] 3306vs br; ν(NH) 3149s; ν[C≡N(b)] 2152w; ν[C≡N(t)] 2120s; ν(C≡N) 1618s. UV-visible (λ_{max}/nm; powder): 430, 658, 809. Magnetic moment: μ_{eff} (295 K) = 3.54 μ_B per molecule.

X-Ray crystal structure determination

Measurements on a green prismatic crystal of **1**, of approximate dimensions 0.22 × 0.20 × 0.20 mm, were made on a Rigaku AFC6R diffractometer with graphite-monochromated Cu-Kα radiation and a rotating anode generator. The data were corrected for Lorentz and polarisation effects and for crystal decay. The structure of **1** was solved by direct methods[37] and refined by full matrix least-squares on F using the teXsan[38] crystallographic software package. The asymmetric unit of the ordered structure contains a cation with pseudo-$P\bar{3}m$ symmetry situated at 0.3513, 0.3271, 0.5000 creating a pseudo-rhombohedral $R\bar{3}m$ symmetry. This symmetry is broken by the locations of the equatorial CN ligands of the cation and by the location of the anion and water molecules. However, a pseudo-inversion at 1/3, 1/3, 0 also relates the 3_2 screw-related molecules at 2/3, 0, 2/3 and 0, 2/3, 1/3. This pseudo-inversion symmetry creates sufficient refinement inconsistencies in an unconstrained refinement (mismatched distances and U_{ij} parameters across the pseudo-inversion centre) to justify a refinement with constraints and restraints. This clearly demonstrated that such features were artifacts of an unconstrained pseudo-centrosymmetric structure refinement.

The program RAELS00[39] was used for the constrained refinement and, in the final cycle, 260 variables were used to refine the 3290 reflections (out of 3937 merged reflections) considered reliably observed with $I > 3\sigma(I)$. All Cl and O atoms were refined as unrestrained isolated atoms. However, the pseudo-centrosymmetric cation was constrained to have 6 identical planar fragments, [N(12), C(102) to C(107)], *etc.*, using a common set of refinable local coordinates defined relative to 6 individually refinable local orthonormal axial systems.[40] Remaining differences in pseudo-centrosymmetrically related bonds in the cation were restrained to approach zero. A 15-parameter rigid-body TLX thermal parameterisation[40] was used for the perchlorate anion. Two 12-parameter TL parameterisations were used for the [N(12) to N(15), C(102) to C(119)] and [N(22) to N(25), C(202) to C(219)] fragments. These were centred on Cu(1) and Cu(2), respectively, and constrained to have equal parameterisations.[41] Pairs of pseudo-centrosymmetrically related atoms in the cation that were not included in the TL parameterisations were constrained to have equal isolated anisotropic atom parameterisations. The water O atoms were refined as isolated anisotropic atoms.

Hydrogen atoms were relocated in geometrically sensible positions after each refinement cycle and given the same thermal parameters as the atoms to which they are attached. Standard deviations are calculated using the inverse of the matrix used for the least-squares and assume the correctness of the various constraints and restraints. Water hydrogens were inserted according to the following hydrogen-bonding pattern: O(2) ··· H–O(1)–H ··· O(4*), O(7) ··· H–O(2)–H ··· O(13*), O(1) ··· H–O(3)–H ··· N(61*), N(31) ··· H–O(4)–H ··· O(6*), N(61) ··· H–O(5)–H ··· O(12), N(41) ··· H–O(6)–H ··· O(14*), N(51) ··· H–O(7)–H ··· O(5*), N(51) ··· H–O(8)–H ··· O(11*). The enantiomorphic structure in $P3_1$ was tested, but refined to give $R(F)$ = 0.068 and GoF = 2.28 for the reflections with $I > 3\sigma(I)$.

Data for compound **5** were collected on a Nonius Kappa CCD diffractometer with graphite-monochromated Mo-Kα radiation. The data were corrected for Lorentz and polarisation effects. The structure was solved by direct methods and refined on F^2 using the SHELX suite of programs.[42] The nitrate counterions were disordered over four equally occupied positions, two of which were related by an inversion centre and required restraints to produce sensible bonding distances, and two which shared the same nitrogen atom and were disordered about another inversion centre. Four solvent water oxygen atoms were assigned, with two [O(3) and O(4)] refined with 70:30 site occupancies and the other two with full occupancy. All non-hydrogen atoms were refined anisotropically, while all non-solvent hydrogen atoms (including the amide hydrogens) were found and placed at calculated positions, but not refined.

Crystal parameters and details of the data collection, solution and refinement for **1** and **5** are summarised in Table 1. ORTEP perspectives of the complexes are presented in Fig. 2 and 3, and selected bond lengths and angles in Tables 2 and 3.

CCDC reference numbers 187746 and 187747.

See http://www.rsc.org/suppdata/dt/b2/b205749m/ for crystallographic data in CIF or other electronic format.

Results and discussion

Synthesis and characterisation

The reaction of [Cu(tpa)(OH$_2$)]$^{2+}$ with half a molar equivalent of K$_3$[Fe(CN)$_6$] afforded [{(tpa)Cu(NC)}$_2$Fe(CN)$_4$]ClO$_4$·6H$_2$O (**1**) as a green powder when conducted in the presence of the oxidising agent K$_2$S$_2$O$_8$. In the absence of K$_2$S$_2$O$_8$, a mixture of **1** and the heptanuclear complex [Fe{(CN)Cu(tpa)}$_6$](ClO$_4$)$_8$·3H$_2$O[22] was obtained. In contrast to this complex, **1** is insoluble in water and the two products could be easily separated. In the case of [{Cu(tren)CN}$_2$Fe(CN)$_4$]ClO$_4$·4H$_2$O (**2**), [Et$_4$N]$_3$[Fe(CN)$_6$] was used instead of K$_3$[Fe(CN)$_6$] and the reaction was carried out in acetonitrile to prevent the "water-assisted" reduction of Fe^{III} to Fe^{II}. [{(H$_2$LN$_4$)$_2$Cu(NC)}$_2$Fe(CN)$_4$]NO$_3$·3H$_2$O (**5**) was obtained as green crystals in aqueous solution and retained the Fe^{III} state whether K$_2$S$_2$O$_8$ was present or not. [{Cu(tpa)NC}$_2$Cr(CN)$_4$]ClO$_4$·8H$_2$O (**3**) and [{Cu([15]aneN$_4$)-NC}$_2$Cr(CN)$_4$]ClO$_4$·4H$_2$O (**4**) were prepared by adding K$_3$[Cr(CN)$_6$] to an aqueous solution of the *in situ*-generated Cu^{II} complex, following the reaction below.

$$[Cr(CN)_6]^{3-} + 2[Cu(L)(OH_2)]^{2+} \longrightarrow [\{Cu(L)NC\}_2Cr(CN)_4]^+$$

This gave a blue–green powder for **3** and a blue-coloured solution for **4**, from which blue platelets were obtained on slow

Table 1 Crystal data for $[\{Cu(tpa)NC\}_2Fe(CN)_4]ClO_4\cdot 8H_2O$ (**1**) and $[\{(H_2LN_4)_2Cu(NC)\}_2Fe(CN)_4]NO_3\cdot 3H_2O$ (**5**)

Empirical formula	$C_{42}H_{52}ClCu_2FeN_{14}O_{12}$	$C_{38}H_{62}Cu_2FeN_{23}O_6$
Formula weight	1163.35	1120.04
Crystal system	Trigonal	Triclinic
Space group	$P3_2$ (#145)	$P\bar{1}$ (#2)
a/Å	12.665(2)	9.8849(1)
b/Å	12.665(2)	11.4809(1)
c/Å	27.860(3)	23.8906(3)
α/°	90	90.392(1)
β/°	90	98.007(1)
γ/°	120	107.933(1)
U/Å^3	3870(1)	2550.85(5)
Z	3	2
ρ_{calc}/g cm^{-3}	1.497	1.458
F_{000}	1797	1166
μ/cm^{-1}	42.69 (Cu-Kα)	11.74 (Mo-Kα)
T/K	296(2)	173(2)
Data measured	6212	41594
Unique data	3845	13921
Observed data	3183 [$I > 3\sigma(I)$]	10336 [$I > 2\sigma(I)$]
Residuals	$R_1 = 0.044$	$R_1 = 0.0525$ (obs. data)
	$R_w = 0.061$	$wR_2 = 0.1466$ (all data)
Goodness of fit indicator	1.71	1.029
$\Delta\rho_{min}$, $\Delta\rho_{max}$/e Å^{-3}	−0.54, 0.56	−1.01, 1.98

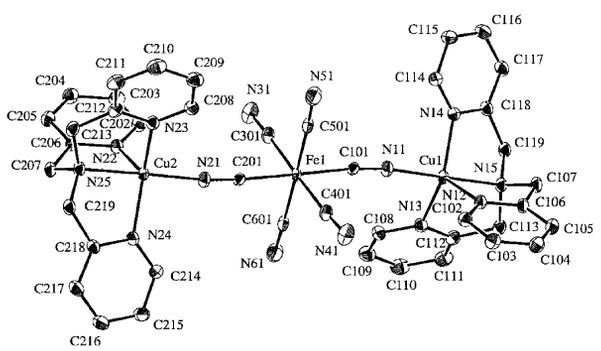

Fig. 2 Thermal ellipsoid diagram of the cation of $[\{Cu(tpa)CN\}_2Fe(CN)_4]ClO_4\cdot 8H_2O$ (**1**) with labelling of selected atoms. Ellipsoids show 30% probability levels. Hydrogen atoms have been deleted for clarity.

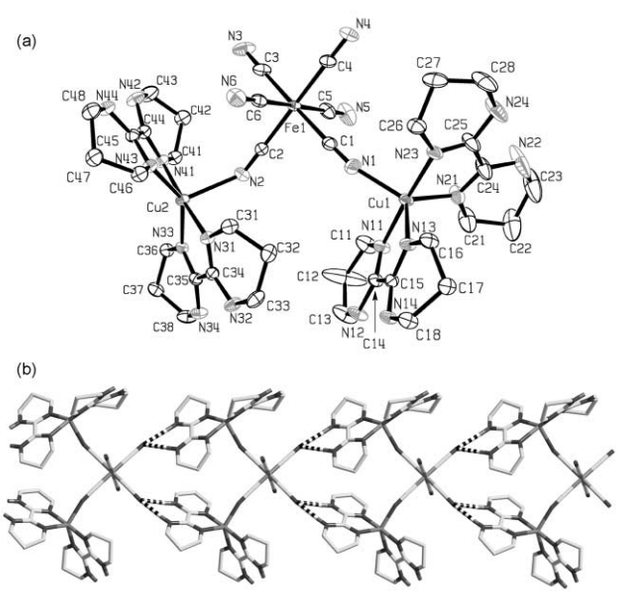

Fig. 3 (a) Thermal ellipsoid diagram of the cation of $[\{(H_2LN_4)_2Cu(NC)\}_2Fe(CN)_4]NO_3\cdot 3H_2O$ (**5**) with atom labelling. Ellipsoids show 50% probability levels. Hydrogen atoms have been deleted for clarity. (b) Hydrogen-bonded chain of trimers which propagates in the y direction; only amidine hydrogens are shown and hydrogen bonds are shown as striped bonds.

Table 2 Selected bond distances (Å) and angles (°) for **1**

Fe(1)–C(201)	1.902(9)	Cu(1)–N(14)	2.035(7)
Fe(1)–C(301)	1.940(9)	Cu(1)–N(13)	2.078(7)
Fe(1)–C(601)	1.936(9)	Cu(1)–N(15)	2.021(8)
Fe(1)–C(101)	1.942(11)	Cu(2)–N(21)	1.943(8)
Fe(1)–C(501)	1.936(9)	Cu(2)–N(22)	2.062(7)
Fe(1)–C(401)	1.934(9)	Cu(2)–N(23)	2.115(7)
Cu(1)–N(11)	1.907(9)	Cu(2)–N(24)	2.021(7)
Cu(1)–N(12)	2.084(7)	Cu(2)–N(25)	2.027(7)
Fe(1)–C(301)–N(31)	177.5(8)	Fe(1)–C(101)–N(11)	180.0(4)
Fe(1)–C(401)–N(41)	177.3(8)	Fe(1)–C(201)–N(21)	174.8(8)
Fe(1)–C(501)–N(51)	175.4(7)	Cu(1)–N(11)–C(101)	171.8(8)
Fe(1)–C(601)–N(61)	178.5(7)	Cu(2)–N(21)–C(201)	172.2(7)

Table 3 Selected bond distances (Å) and angles (°) for **5**

Fe(1)–C(1)	1.927(3)	Cu(1)–N(1)	2.049(3)
Fe(1)–C(2)	1.929(3)	Cu(1)–N(11)	1.975(3)
Fe(1)–C(3)	1.935(3)	Cu(1)–N(13)	2.060(2)
Fe(1)–C(4)	1.940(3)	Cu(1)–N(21)	2.037(3)
Fe(1)–C(5)	1.931(3)	Cu(1)–N(23)	1.965(2)
Fe(1)–C(6)	1.939(3)	Cu(2)–N(2)	2.241(3)
Cu(2)–N(31)	1.975(2)	Cu(2)–N(41)	1.978(2)
Cu(2)–N(33)	2.014(2)	Cu(2)–N(43)	2.008(2)
Fe(1)–C(3)–N(3)	178.5(3)	N(1)–C(1)–Fe(1)	176.3(3)
Fe(1)–C(4)–N(4)	178.8(3)	N(2)–C(2)–Fe(1)	177.7(3)
Fe(1)–C(5)–N(5)	178.6(4)	Cu(1)–C(1)–N(1)	161.9(3)
Fe(1)–C(6)–N(6)	179.5(3)	Cu(2)–C(2)–N(2)	137.2(2)

evaporation at room temperature. Microanalyses were consistent with the given formulations, while electron microprobe analysis showed the uniform presence of Fe/Cr, Cu and Cl, in the approximate ratio 1:2:1.

For complexes **1**–**3** and **5**, two bands were observed in the ν_{CN} stretching region. The higher frequency ν_{CN} stretching vibrations, located at 2158 (**1**), 2148 (**2**), 2178 (**3**) and 2152 (**5**) cm^{-1}, are assigned to the intermetallic $M^{III}C{\equiv}NCu^{II}$ bonds, ν[C≡N(b)]. The other bands at 2123 (**1**), 2101 (**2**), 2129 (**3**) and 2120 (**5**) cm^{-1} are assigned to terminal C≡N stretching modes, ν[C≡N(t)], since they correspond well with the terminal ν_{CN} vibrations of potassium ferricyanide (ν_{CN} 2115 cm^{-1}) and potassium hexacyanochromate (ν_{CN} 2131 cm^{-1}). In the case of **4**, an intense band at 2128 cm^{-1}, attributed to a terminal ν(C≡N) mode, masks the intermetallic ν(C≡N). The presence of the tpa ligand in **1** and **3** is confirmed by skeletal vibrations of the pyridyl ring observed in the 1400–1610 cm^{-1} range, while in

the case of **2** and **4**, N–H vibrations at 3325 and 3267 cm^{-1} (**2**) and 3234 cm^{-1} (**4**) indicate the presence of the amine ligands tren and [15]aneN_4. For **5**, bands from the NH and C=N groups in H_2LN_4 were evident.

Mössbauer spectroscopy

The Mössbauer spectra of **1** (77), **2** (293) and **5** (77 K) show strong doublets with quadrupole splittings (ΔE_Q) of 2.29, 1.027 and 0.833 mm s^{-1}, respectively. The similarity in the isomer shifts for **1**, **2** and **5** (−0.080, −0.157 and −0.060 mm s^{-1}, respectively) to those observed for $K_4[Fe(CN)_6]$, (δ = 0.04 mm s^{-1}, ΔE_Q = 0.0 mm s^{-1}) and $K_3[Fe(CN)_6]$ (δ = 0.0 mm s^{-1}, ΔE_Q = 0.47 mm s^{-1}),[43] means that the iron oxidation state cannot be assigned on this basis alone. However, the fact that the spectra of **1**, **2** and **5** display well-resolved quadrupole splitting is consistent with the presence of an Fe^{III} cyanometallate core.

Electronic spectra

The solution UV-visible spectra of **1** and **2** exhibit bands at 420 and 426 nm, respectively, which can be ascribed to a Fe^{III} (t_{2g}) ⟶ $L(CN^-)_g$ symmetry-forbidden charge transfer, as found in the spectrum of ferricyanide.[44] For the Cr^{III} complexes **3** and **4**, the expected Cr^{III} d–d transitions are masked. The spectra of complexes **1**, **2** and **3** show bands at 834, 811 and 790 nm, respectively, which are assigned to a d–d transition in a Cu^{II} centre in trigonal bipyramidal (TBP) geometry.[45] Shoulders in the 600–665 nm region indicate some distortion of the Cu^{II} geometry towards square planar (SP).[45,46] The spectrum of the related Fe^{III} trinuclear Schiff-base (L) complex, $[\{Cu(L)NC\}_2Fe(CN)_4](ClO_4)\cdot 2CH_3OH\cdot 12H_2O$, shows bands at 380 and 620 nm, the latter being due to Cu^{II} in distorted SP geometry.[32] For **4**, the solution spectrum shows a band at 592 nm that is typical of a d–d transition for a SP or octahedral Cu^{II} complex.[47]

The solid-state spectra of **1**, **2** and **3** are similar to the solution spectra, apart from slight shifts and general broadening of the Cu^{II} d–d bands. Cu^{II} adopts a TBP stereochemistry in solution and solid state. In the case of **1**, the X-ray structure confirms a distorted TBP geometry around the Cu^{II} centres (see below). The spectrum of complex **5** shows bands at 658 and 809 nm, in agreement with the distorted SP geometry around the Cu^{II} centre. The solid-state spectrum of **4** differs slightly from the solution spectrum. A more prominent band is found at 380nm, which could be due to a metal-to-metal charge transfer; the main Cu^{II} d–d transition has shifts from 592 (solution) to 606 nm (solid state); and a shoulder appears at 830 nm. The Cu^{II} centre could be octahedral in solution and SP in the solid state, where two bands are expected (at ~600 and 800–1100 nm), as found for many other SP Cu^{II} complexes.[47]

Crystal structures

The ORTEP view of $[\{Cu(tpa)NC\}_2Fe(CN)_4]ClO_4\cdot 6H_2O$ (**1**) shown in Fig. 2, confirms that the complex cation is a discrete linear trinuclear unit in which the two $[Cu(tpa)]^{2+}$ moieties bind to two axial cyanides, thereby adopting a *trans* orientation. The four terminal cyanides occupy the four equatorial positions around the iron core. As was found for discrete heptanuclear complexes, the geometry around the Fe^{III} centre shows little distortion from octahedral geometry, *viz*. C–Fe–C *trans* angles of 178.7(8)–180.0(4)° and C–Fe–C *cis* angles of 84.6(3)–95.4(4)°. The Fe–C bond distances vary between 1.902(9) and 1.942(11) Å which, along with interatomic angles around the core, are consistent with those found in other discrete (*e.g.* see ref. 22 and 25) and polymeric (*e.g.* see ref. 10 and 14) hexacyanoferrate(II/III) complexes. The Cu–N(cyano) distances range from 1.907(9) to 1.943(8) Å and compare well to values reported in Fe–CN–Cu assemblies.[18,22,26] The Cu–N–C(cyano) angles (av. 172°) are similar to those found in other discrete molecules,[18] but different to the corresponding angles in closely related discrete trinuclear complexes, *viz*. Cu–N–C(CN) is 148(av.), 144.1 and 148(av.)° in $[\{Cu(L)NC\}_2Fe(CN)_4](ClO_4)\cdot 2CH_3OH\cdot 12H_2O$, $[\{Cu(tren)NC\}_2Fe(CN)_4]\cdot 12H_2O$ and $[\{Cu(L)_2NC\}_2Fe(CN)_4]\cdot 2CH_3OH\cdot H_2O$ [L = *N*,*N*′-bis(2-pyridylimine)propane-1,3-diamine], respectively.[25,32] This is surprising given that all three complexes consist of discrete trinuclear units with *trans*-oriented SP or TBP Cu^{II} centres connected *via* a hexacyanoferrate and that the cyanide ligand occupies an axial site in the Cu^{II} coordination sphere.

The Cu^{II} geometry in **1** is distorted TBP. The τ value describing the geometry around the Cu^{II} ions, calculated according to Addison and co-workers,[48] is 0.90, for Cu(1) and 0.80, for Cu(2) (where τ = 1.00 for TBP and 0.00 for SP). The pyridyl nitrogens on the tpa occupy the equatorial positions and the amine nitrogen an axial position *trans* to the cyano nitrogen [angle close to linear, 178.7° in Cu(1) and 177.7° in Cu(2)]. This characteristic is common to Fe–C≡N–Cu complexes with TBP Cu^{II} geometry.[18] In the case of the trinuclear complex $[\{Cu(tren)CN\}_2Fe(CN)_4]\cdot 12H_2O$, the (amine)N–Cu–N(cyano) angle (169.4°), however, shows more deviation from linearity, even though the less bulky tren ligand would be expected to impart less distortion than tpa. As is typical for Cu^{II}–tpa complexes,[49] the copper centres in **1** sit outside the plane formed by the pyridyl nitrogens toward the bridging cyano group by 0.271 Å for Cu(1) and 0.262 Å for Cu(2). These values are slightly lower than those observed in the heptanuclear complex $[\{Cu(tpa)CN\}_6Fe]^{8+}$,[22] as might be expected given that, in this case, greater steric interactions are anticipated between adjacent $[Cu(tpa)]^{2+}$ moieties and, surprisingly, the mononuclear complex $[Cu(tpa)CN]ClO_4$[50] shows a displacement (0.337 Å) that is greater than that in either type of heterometallic complex.

The structure of $[\{(H_2LN_4)_2Cu(NC)\}_2Fe(CN)_4]NO_3\cdot 3H_2O$ (**5**) is shown in Fig. 3. Although this compound is also trinuclear, the two copper species $\{[Cu(H_2LN_4)_2]^{2+}\}$ are now coordinated to *cis*-disposed cyanides on the central $[Fe(CN)_6]^{3-}$ moiety. Again, the $[Fe(CN)_6]^{3-}$ core is close to regular octahedral, with C–Fe–C *trans* angles ranging between 176.6(1) and 179.1(1)°, the C–Fe–C *cis* angles being 87.4(2)–92.0(1)° and the Fe–C bond lengths lying between 1.927(3) and 1.940(3) Å, consistent with **1**.

The sterically less favoured *cis* bonding of the $Cu(H_2LN_4)_2^{2+}$ moieties in **5** does, however, induce changes to the Cu–N(cyano) bonding when compared to the *trans* structure of **1**. The Cu–N(cyano) bonds are longer than in **1**, with the bond to Cu(2) being longer [2.241(3) Å] than the corresponding Cu–N(cyano) bond to Cu(1) [2.049(3) Å]. The angle at the cyanide nitrogen atom bonded to Cu(2) is also considerably more distorted from linear [137.2(2)°] than is the angle at Cu(1) [161.9(3)°].

One copper atom [Cu(1)] is in a slightly distorted TBP geometry (τ = 0.83) in which the bridging cyano ligand occupies an equatorial position on the metal coordination sphere and the chelating amidine ligands span equatorial and axial positions [see Fig. 3(a)]. The geometry around Cu(2), however, is intermediate between TBP and SP (τ = 0.52). The H_2LN_4 ligands all show chair conformations and are neutral, with all the amidine hydrogen atoms observed in the structure solution.

The presence of hydrogen bond donor groups on the H_2LN_4 ligands and cyano acceptor groups leads to extensive hydrogen bonding within the structure, details of which are given in Table 4. The intercalated water molecules and the nitrate counterions are also involved. One H_2LN_4 ligand on each of the copper atoms hydrogen bonds in a bifurcated manner *via* its two amidine hydrogens, each bonding to an uncoordinated cyanide nitrogen atom of an adjoining cluster, which is translated a unit cell length along the $-y$ direction from the first. The N(12)–H(12)/N(14)–H(14) amidine ligand hydrogen bonds to the N(4) cyanide atom, while the N(32)–H(32)/N(34)–H(34) amidine ligand hydrogen bonds to the N(3) cyanide atom. This

Table 4 Hydrogen bonding distances (Å) and angles (°) in **5**

Interaction	D–H	H–A	D–A	D–H–A
N(12)–H(12)–N(4)[a]	0.880	2.011	2.888(4)	173.6
N(14)–H(14)–N(4)[a]	0.880	2.120	2.998(4)	175.7
N(32)–H(32)–N(3)[a]	0.880	2.037	2.914(4)	174.2
N(34)–H(34)–N(3)[a]	0.880	2.066	2.945(4)	177.8
N(42)–H(42)–O(1)[b]	0.880	2.111	2.941(4)	156.9
N(44)–H(44)–O(1)[b]	0.880	2.062	2.937(3)	172.7
O(1)–N(6)			2.731(4)	
O(1)–O(2)			2.817(4)	
O(1)–O(2)[c]			2.751(4)	
N(22)–H(22)–O(3)[d]	0.880	2.212	3.088(6)	173.8
N(24)–H(24)–O(3)[d]	0.880	1.937	2.806(6)	169.1
N(24)–H(24)–O(4)[d]	0.880	2.227	2.90(1)	132.7
O(3)–N(5)			2.791(7)	
O(4)–N(5)			2.81(1)	
O(3)–O(62)[e]			2.45(1)	
O(3)–O(63)[d]			2.78(1)	
O(4)–O(62)[e]			2.95(2)	
O(4)–O(63)[d]			2.82(2)	

[a] $x, y + 1, z$; [b] $2 - x, 1 - y, 1 - z$; [c] $1 - x, 1 - y, 1 - z$; [d] $1 - x, 1 - y, - z$; [e] $1 + x, 1 + y, z$.

hydrogen bonding generates a chain of connected clusters parallel to the *y* direction [Fig. 3(b)].

The other two unique H_2LN_4 ligands also participate in hydrogen bonding. The N(42)–H(42)/N(44)–H(44) ligand forms a bifurcated hydrogen bond to one of the intercalated water molecules [O(1)]. This water is also involved in a hydrogen bonding interaction to the N6 cyanide atom of an adjoining cluster, as well as forming part of a $O(1)_2O(2)_2$ hydrogen-bonded rhombus which is disposed about a center of symmetry. This $(H_2O)_4$ rhombus thus connects four separate clusters—each of the two O(1) water molecules accepts a bifurcated hydrogen bond from an H_2LN_4 ligand of one cluster and makes a hydrogen bond to a cyanide of another cluster.

The remaining H_2LN_4 ligand [N(22)–H(22)/N(24)–H(24)] hydrogen bonds in a bifurcated manner to the partially occupied O(3) water, while the O(4) water, also partially occupied, only hydrogen bonds to the N(24)–H(24) moiety. These two partially occupied water positions are also both within hydrogen bonding distance of the N(5) cyanide atom of a separate cluster, as well as the two nitrate anions disordered about the N(61) atom. Thus, all amidine ligands participate in bifurcated hydrogen bonds, and all non-bridging cyano nitrogens accept hydrogen bonds. All the intercalated water molecules are also hydrogen bonding, while only two of the four positions of the disordered nitrate anion are within hydrogen bonding distance to likely donor groups.

Magnetic properties

The room temperature value of χT for **1** is 1.403 cm³ K mol^{-1} which, due to spin–orbit effects, is higher than the spin-only value of 1.125 cm³ K mol^{-1} expected for a magnetically dilute spin system (S_{Cu}, S_{Fe}, S_{Cu}) = ($\frac{1}{2}$, $\frac{1}{2}$, $\frac{1}{2}$), calculated assuming g = 2.00. As the temperature is decreased, the magnetic behaviour is Curie-like until about 90 K (Fig. 4). Below this temperature, χT increases steadily, reaching a maximum of 1.863 cm³ K mol^{-1} at 5.0 K, in accordance with a weakly ferromagnetically coupled trinuclear system consisting of one low spin Fe^{III} ($S = \frac{1}{2}$) and two Cu^{II} ($S = \frac{1}{2}$) ions. The ability of the Cu^{II}–N≡C–Fe^{III} bridging unit to mediate ferromagnetic interactions can be rationalised in terms of the strict orthogonality of the magnetic orbitals of the Fe^{III} [$(t_{2g})^5$] and Cu^{II} [$(e_g)^3$] centres, an arrangement which normally gives rise to ferromagnetic coupling.[7,26]

The magnetic susceptibility data are reproduced well by using the exchange spin Hamiltonian (eqn. 1) for a discrete trinuclear

$$\boldsymbol{H} = -2J_{12}(\boldsymbol{S}_{Cu(1)}\boldsymbol{S}_{Fe} + \boldsymbol{S}_{Cu(2)}\boldsymbol{S}_{Fe}) - 2J_{13}(\boldsymbol{S}_{Cu(1)}\boldsymbol{S}_{Cu(2)}) \quad (1)$$

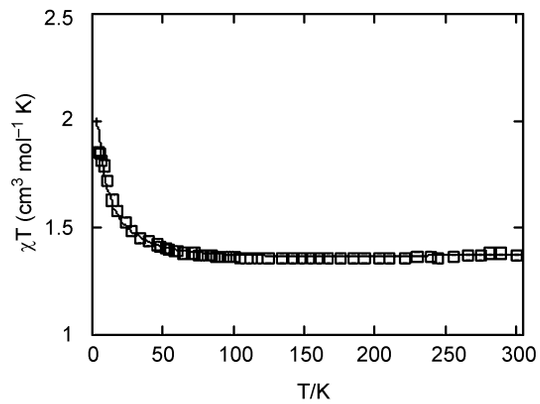

Fig. 4 Plot of χT *vs.* T for [{(tpa)Cu(NC)}$_2$Fe(CN)$_4$]ClO_4·6H_2O (**1**), in a field of 1 T. The solid line was calculated using eqn. 1 and the parameter values are given in the text.

structure of {Cu^{II}–Fe^{III}–Cu^{II}}, in which we assume a {$S = \frac{1}{2}$}–{$S = \frac{1}{2}$}–{$S = \frac{1}{2}$} spin system.

Spin–orbit and ligand-field effects for Fe^{III} are not treated explicitly as was done by Gupta *et al.*[51] for a related ferromagnetically coupled linear trinuclear complex, [{Cu^{II}(im)}$_2$-Fe^{III}(TPP)]$B_{11}CH_{12}$·5THF. The present g values for the Fe^{III} and Cu^{II} centres are assumed equal and their values reflect spin–orbit effects on the metal centres. The best fit parameters are g = 2.16, J_{12} = 4.3 cm^{-1}, and J_{13} = −0.18 cm^{-1} based on a symmetric linear trinuclear structure, assuming that the interaction between Cu^{II} centres is weak ($J_{13} << J_{12}$).

In the case of **2**, for which we do not have a crystal structure, the χT value of 1.585 cm³ K mol^{-1} at 290 K is higher than the expected spin-only value of 1.125 cm³ K mol^{-1} (see above). As the temperature is decreased, the χT value decreases slowly to a value of 1.506 cm³ K mol^{-1} at about 140 K (Fig. 5). As the

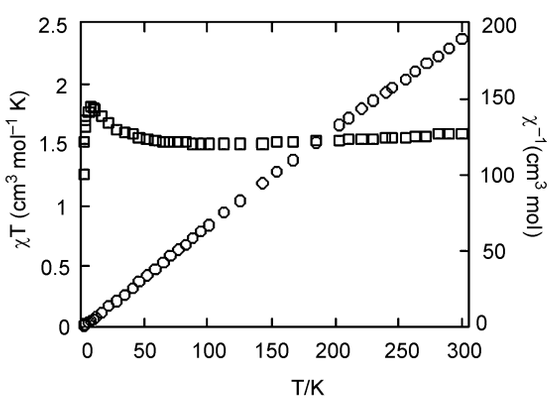

Fig. 5 Plots of χT *vs.* T and $1/\chi$ *vs.* T for [{Cu(tren)CN}$_2$Fe(CN)$_4$]-ClO_4·4H_2O (**2**), in a field of 1 T.

temperature is decreased further, the magnetic moment reaches a broad minimum at *ca.* 100 K, then shows a steady increase to a maximum of 1.806 cm³ K mol^{-1} at 8.0 K. Below this temperature, χT "turns over" and rapidly falls to a minimum value of 1.256 cm³ K mol^{-1} at 2.0 K. As is the case for **1**, the magnetic behaviour between 8.0–90 K, is consistent with a ferromagnetically coupled trinuclear species with one low spin Fe^{III} ($S = \frac{1}{2}$) and two Cu^{II} ($S = \frac{1}{2}$) ions. In this temperature range, the magnetic susceptibility obeys the Curie–Weiss law, with a Weiss constant of θ = +2.3 K. In contrast to **1**, however, the susceptibility behaviour above ~140 K for **2** yields a Weiss constant of θ = −16.7 K. A negative θ value could originate from spin–orbit effects on Fe^{III} or result from inter-complex ferrimagnetic chain-like interactions, which characteristically yield broad minima in χT.[7] Interestingly, a broad minimum in χT was also evident at ~130K in the imidazolate-bridged Cu_2–Fe porphyrin[51] and not simulated, even when {Fe^{III}, t_{2g}^5} ligand field/

spin–orbit and second order Zeeman (Fe^{III} and $2Cu^{II}$) corrections were made to the observed χ values. The low temperature (<8 K) decrease in χT in that case was ascribed to inter complex (Cu–Cu) interactions noted in the chain-like structure. Such could be the case here. Zero-field splitting of the $S = 3/2$ ground state could also be responsible for the sharp decrease in μ at lower temperatures. At a molecular level, the linearity or non-linearity of the Cu^{II}–Fe^{III}–Cu^{II} linkage (linear in **1** and bent for the Fe^{II} analogue of **2**[25] and a Schiff-base complex[32]) will influence the superexchange mechanism and the resultant sign of J. The χT *vs.* T data for **2** could not be simulated using eqn. 1, whatever the combination of J_{12}, J_{13}, χ(TIP) or $(T - \theta)$ was employed, θ allowing for the inter-complex coupling and giving the decrease in χT at very low temperatures.

The χT *vs.* T data for the *cis*-CN-bridged complex (**5**) were identical for two separate samples (Fig. 6). They show essentially Curie-like susceptibility behaviour in which the corresponding χT (per molecule) values change only slightly from 1.585 cm^3 K mol^{-1} at 300 K to 1.532 cm^3 K mol^{-1} at ~40 K, before rising gently to a maximum of 1.576 cm^3 K mol^{-1} at 12.5 K. A sharper decrease then occurs, reaching 1.462 cm^3 K mol^{-1} at 4.2 K. The data are broadly similar to those of **1** and the imidazolate-bridged Cu_2–Fe porphyrin,[51] but with a less steep rise in χT occurring at low temperature. A reasonable fit of the complete data was obtained using the parameter values g = 2.31, $J_{12} = +1.95$ cm^{-1}, $J_{13} = -2.1$ cm^{-1}, TIP(total) = 220×10^{-6} cm^3 mol^{-1} and $\theta = 0.02$ K. The J_{12} (CuFe) and J_{13} (CuCu) values are equal, opposite in sign and small. It is likely that the negative J_{13} value is larger than in **1** because of the *cis* disposition of the Cu–NC–Fe–CN–Cu bridges and the influence that this has on magnetic orbital overlap involving Fe (t_{2g}) and Cu (e_g) orbitals *via* the cyanide p-orbitals. The bent Cu–N–C angles, around Cu(1) and Cu(2), combined with the different coordination geometries of the Cu centres (*vide infra*), might play a part in the overall weakly coupled behaviour.

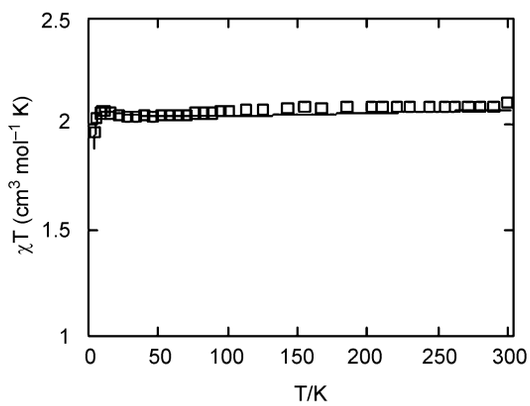

Fig. 6 Plot of χT *vs.* T for $[\{(H_2LN_4)_2Cu(NC)\}_2Fe(CN)_4]NO_3 \cdot 3H_2O$ (**5**), in a field of 1 T. The solid line was calculated using eqn. 1 and the parameter values are given in the text.

For **3**, the χT value at room temperature of 2.443 cm^3 K mol^{-1} is slightly lower than the spin-only value of 2.623 cm^3 K mol^{-1} expected for a magnetically dilute spin system $[2(S_{Cu}), S_{Cr}] = (\frac{1}{2}, \frac{3}{2})$. In Fig. 7, it can be seen that as the temperature is decreased, there is a steady increase in χT until a maximum of 4.020 cm^3 K mol^{-1} is reached at 16.2 K. This value correlates quite well to the expected spin-only value of 4.377 cm^3 K mol^{-1} for a fully ferromagnetically coupled trinuclear system with one Cr^{III} ion ($S = \frac{3}{2}$, $g = 2.00$) and two Cu^{II} ions ($S = \frac{1}{2}$, $g = 2.00$). On further lowering of the temperature, the χT values "turn over", decreasing to a final value of 3.714 cm^3 K mol^{-1} at 4.5 K, probably due to zero-field splitting of the $S = 5/2$ ground state and thermal depopulation of closely spaced Zeeman (M_S) levels. The magnetic behaviour above 16 K suggests an intramolecular ferromagnetic interaction between the Cr^{III} and surrounding Cu^{II} ions, mediated through the cyanide bridge. In accordance with this, the magnetic susceptibility obeys the Curie–Weiss law, with a positive Weiss constant of $\theta = +19.7$ K. As in complexes **1** and **2**, the ferromagnetic interaction can be rationalised in terms of the strict orthogonality of the magnetic orbitals of the Cr^{III} [$(t_{2g})^3$] and Cu^{II} [$(e_g)^3$] ions.

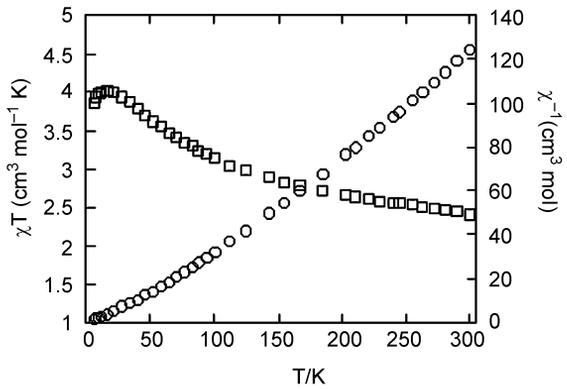

Fig. 7 Plots of χT *vs.* T and $1/\chi$ *vs.* T for $[\{Cu(tpa)NC\}_2Cr(CN)_4]ClO_4 \cdot 8H_2O$ (**3**), in a field of 1 T.

Attempts were made to analyse the magnetic susceptibility data using the spin Hamiltonian (eqn. 1) for a discrete trinuclear $\{Cu^{II}$–Cr^{III}–$Cu^{II}\}$ structure with an $\{S = \frac{1}{2}\}$–$\{S = \frac{3}{2}\}$–$\{S = \frac{1}{2}\}$ spin system.

The fits obtained thus far are poor and not shown in Fig. 7. The fact that χT at 300 K is lower than the spin-only (non-coupled) value suggests that some contaminating species may be present.

For **4**, the χT value at 290 K of 2.941 cm^3 K mol^{-1} is slightly higher than the spin-only value of 2.623 cm^3 K mol^{-1} expected for a magnetically dilute $(S_{Cu}, S_{Cr}, S_{Cu}) = (\frac{1}{2}, \frac{3}{2}, \frac{1}{2})$ spin system. As the temperature is decreased, there is a slow and steady increase in χT to 50 K, and then a more rapid increase below this temperature, until a maximum of 3.714 cm^3 K mol^{-1} is reached at 6 K. The χT value at this temperature is lower than expected (4.377 cm^3 K mol^{-1}) for a fully ferromagnetically coupled trinuclear system. When the temperature is lowered further, the χT values begin to decrease a little, again probably due to Zeeman level depopulation effects combined with zero-field splitting effects, as in **3**. Above 6 K, an intramolecular ferromagnetic interaction between the Cr^{III} and surrounding Cu^{II} ions is mediated through the cyanide bridges. In this region, the magnetic susceptibility obeys the Curie–Weiss law, with a positive Weiss constant ($\theta = +2.4$ K). As can be seen in Fig. 8, the magnetic susceptibility data for **4** are reproduced well by using the spin Hamiltonian (eqn. 1) for a discrete trinuclear $\{S = \frac{1}{2}\}$–$\{S = \frac{3}{2}\}$–$\{S = \frac{1}{2}\}$ spin system. The best-fit parameters

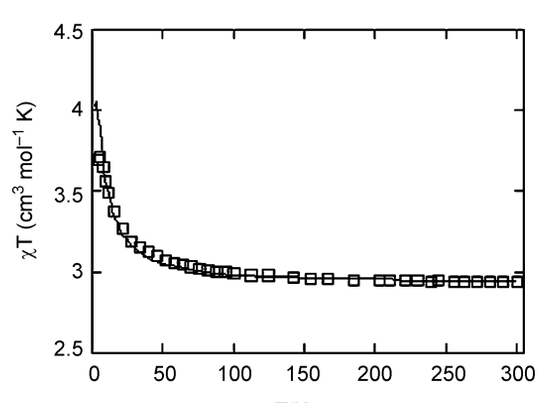

Fig. 8 Plot of χT *vs.* T for $[\{Cu([15]aneN_4)NC\}_2Cr(CN)_4]ClO_4 \cdot 4H_2O$ (**4**), in a field of 1 T. The solid line was calculated using eqn. 1 and the parameter values are given in the text.

are $g = 2.1$, $J_{CuCr} = 1.31$ cm^{-1}, $J_{CuCu} = 0$ cm^{-1} and TIP = 100×10^{-6} cm^3 mol^{-1} per molecule. The agreement is good, except that the maximum in χT is not reproduced by this simple model, which does not include ZFS terms. The J value confirms an intramolecular ferromagnetic coupling between the Cu^{II} and Cr^{III} centres.

Acknowledgements

This work was supported by the Australian Research Council. R. J. P. was the recipient of a Monash Graduate Scholarship. Mr K. J. Berry is thanked for theoretical input. We thank Professor C. A. Reed and Dr P. D. W. Boyd for discussions on their unpublished work on related $Cu^{II}Fe^{III}Cu^{II}$ systems.

References

1 O. Kahn *Molecular Magnetism*, VCH, Weinheim, Germany, 1993.
2 (*a*) V. Gadet, M. Bujoli-Doeuff, L. Force, M. Verdaguer, K. El Malkhi, A. Deroy, J. P. Besse, C. Chappert, P. Veillet, J. P. Renard and P. Beauvillain, in *Magnetic Molecular Materials*, ed. D. Gatteschi, O. Kahn, J. S. Miller and F. Palacio, NATO ASI Ser., Ser. E, Kluwer Academic, Dordrecht, 1991, vol. 198, p. 281; (*b*) M Verdaguer, A. Bleuzen, C. Train, R. Garde, F. Fabrizi de Biani and C. Desplaches, in *Molecular-Organic and Organic Molecular Magnets*, ed. P. Day and A. E. Underhill, Royal Society of Chemistry, Cambridge, 2000, p. 105.
3 K. R. Dunbar and R. A Heintz, *Prog. Inorg. Chem.*, 1997, **45**, 283.
4 H. Vahrenkamp, A. Geiss and G. N. Richardson, *J. Chem. Soc., Dalton Trans.*, 1997, 3643.
5 T. Mallah, A. Marvilliers and E. Riviere, in *Molecular-Organic and Organic Molecular Magnets*, ed. P. Day and A. E. Underhill, Royal Society of Chemistry, Cambridge, 2000, p. 302.
6 (*a*) W. R. Entley and G. S. Girolami, *Inorg. Chem.*, 1994, **33**, 5165; (*b*) W. R. Entley and G. S. Girolami, *Science*, 1995, **268**, 397.
7 O. Kahn, *Adv. Inorg. Chem.*, 1995, **43**, 179.
8 O. Sato, Y. Einaga, A. Fujishima and K. Hashimoto, *Inorg. Chem.*, 1999, **38**, 4405.
9 M. Ohba and H. Okawa, *Coord. Chem. Rev.*, 2000, **198**, 313 and references therein.
10 (*a*) H. Miyasaka, N. Matsumoto, N. Re, E. Gallo and C. Floriani, *Inorg. Chem.*, 1997, **36**, 670; (*b*) H. Miyasaka, H. Ieda, N. Matsumoto, N. Re, R. Crescenzi and C. Floriani, *Inorg. Chem.*, 1998, **37**, 255 and references therein.
11 (*a*) J. Larionova, J. Sanchiz, S. Gohlen, L. Ouahab and O. Kahn, *Chem. Commun.*, 1998, 953; (*b*) J. Larionova, O. Kahn, S. Gohlen, L. Ouahab and R. Clerac, *J. Am. Chem. Soc.*, 1999, **121**, 3349.
12 (*a*) E. Colacio, J. M. Dominguez-Vera, M. Ghazi, R. Kivekäs, F. Lloret, J. M. Moreno and H. Stoeckli-Evans, *Chem. Commun.*, 1999, 987; (*b*) E. Colacio, J. M. Dominguez-Vera, M. Ghazi, R. Kivekäs, J. M. Moreno and A. Pajuner, *J. Chem. Soc., Dalton Trans.*, 2000, 505.
13 J. A. Smith, J.-R. Galan-Mascaros, R. Clerac and K. R. Dunbar, *Chem. Commun.*, 2000, 1077.
14 (*a*) H.-Z Kou, D.-Z Liao, P. Cheng, Z.-H. Jiang, S.-P. Yan, G.-L. Wang, X.-K. Yao and H.-G. Wang, *J. Chem. Soc., Dalton Trans.*, 1997, 1503; (*b*) H.-Z. Kou, W.-M. Bu, S. Gao, D.-Z. Liao, Z.-H. Jiang, S.-P. Yan, Y.-G. Fan and G.-L. Wang, *J. Chem. Soc., Dalton Trans.*, 2000, 2996; (*c*) H.-Z. Khou, S. Gao, B.-Q. Ma and D.-Z Liao, *Chem. Commun.*, 2000, 1309.
15 T. Lu, H. Xiang, C. Su, P. Cheng, Z. Mao and L. Ji, *New J. Chem.*, 2001, **25**, 216.
16 M. J. Gunter, K. J. Berry and K. S. Murray, *J. Am. Chem. Soc.*, 1984, **106**, 4227.
17 J. P. Collman, L. Fu, P. C. Hermann and X. Zhang, *Science*, 1997, **275**, 949.
18 (*a*) S. C. Lee, M. J. Scott, K. Kauffmann, E. Münck and R. H. Holm, *J. Am. Chem. Soc.*, 1994, **116**, 401; (*b*) M. J. Scott and R. H. Holm, *J. Am. Chem. Soc.*, 1994, **116**, 11357.
19 D. M. Corsi, N. N. Murthy, V. C. Young, Jr. and K. D. Karlin, *Inorg. Chem.*, 1999, **38**, 848.
20 T. Mallah, C. Auberger, M. Verdaguer and P. Veillet, *Chem. Commun.*, 1995, 61.
21 A. Scuiller, T. Mallah, M. Verdaguer, A. Nivorozkhin, J. Tholence and P. Veillet, *New J. Chem.*, 1996, **20**, 1.
22 R. J. Parker, D. C. R. Hockless, B. Moubaraki, K. S. Murray and L. Spiccia, *Chem. Commun.*, 1996, 2789.
23 K. Van Langenberg, S. R. Batten, K. J. Berry, D. C. R. Hockless, B. Moubaraki and K. S. Murray, *Inorg. Chem.*, 1997, **36**, 5006.
24 J. L. Heinrich, P. A Berseth and J. R. Long, *Chem. Commun.*, 1998, 1232.
25 (*a*) Z.-L. Lu, C.-Y. Duan, Y. P. Tian, Z.-W. Wu, J.-J. You, Z.-Y. Zhou and T. C. W. Mak, *Polyhedron*, 1997, **16**, 909; (*b*) J. Zou, Z. Xu, X. Huang, W.-L Zhang, X.-P. Shen and Y.-P. Yu, *J. Coord. Chem.*, 1997, **42**, 55.
26 M. Verdaguer, A. Bleuzen, V. Marvaud, J. Vaissermann, M. Seuleiman, C. Desplanches, A. Scuiller, C. Train, R. Garde, G. Gelly, C. Lomenech, I. Rosenman, P. Veillet, C. Cartier and F. Villain, *Coord. Chem. Rev.*, 1999, **190–192**, 1023.
27 (*a*) Z. J. Zhong, H. Seino, Y. Mizobe, M. Hidai, A. Fujishima, S. Ohkoshi and K. Hashimoto, *J. Am. Chem. Soc.*, 2000, **122**, 2952; (*b*) Z. J. Zhong, H. Seino, Y. Mizobe, M. Hidai, M. Verdaguer, S. Ohkoshi and K. Hashimoto, *Inorg. Chem.*, 2000, **39**, 5095.
28 J. Larianova, M. Gross, M. Pilkington, H. Audres, H. Stoeckli-Evans, H. U. Güdel and S. Decurtins, *Angew. Chem., Int. Ed.*, 2000, **39**, 1605.
29 R. J. Parker, L. Spiccia, K. J. Berry, G. D. Fallon, B. Moubaraki and K. S. Murray, *Chem. Commun.*, 2001, 333.
30 (*a*) R. J. Parker, L. Spiccia, S. R. Batten, J. D. Cashion and G. D. Fallon, *Inorg. Chem.*, 2001, **40**, 4696; (*b*) R. J. Parker, L. Spiccia, B. Moubaraki, K. S. Murray, D. C. R. Hockless, A. D. Rae and A. C. Willis, *Inorg. Chem.*, 2002, **41**, 2489.
31 L. Spiccia, K. S. Murray and J. F. Young, *Inorg. Synth.*, in press.
32 N. Mondal, S. Mitra and G. Rosair, *Polyhedron*, 2001, **20**, 2473.
33 (*a*) G. Anderegg and F. Wenk, *Helv. Chim. Acta*, 1967, **50**, 2330; (*b*) J. W. Canary, Y. Wang and R. Roy Jr., *Inorg. Synth.*, 1998, **32**, 70.
34 M. G. Burnett, V. McKee and S. M. Nelson, *J. Chem. Soc., Dalton Trans*, 1981, 1492.
35 P. K. Mascharak, *Inorg. Chem.*, 1986, **25**, 247.
36 J. H. Bigelow, *Inorg. Synth.*, 1947, **2**, 203.
37 A. Altomare, M. Cascarano, C. Giacovazzo and A. Guagliardi, *J. Appl. Crystallogr.*, 1993, **26**, 343.
38 teXan, Crystal Structure Analysis Package, Molecular Structure Corporation, The Woodlands, TX, USA, 1985 and 1992.
39 A. D. Rae, RAELS00, Australian National University, Canberra, Ausralia, 2000.
40 A. D. Rae, *Acta Crystallogr., Sect. A*, 1975, **31**, 560–570.
41 A. D. Rae, *Acta Crystallogr., Sect. A*, 1996, **52**, C44.
42 G. M. Sheldrick, SHELX-97, Program for Crystal Structure Refinement, University of Göttingen, Germany, 1997.
43 N. N. Greenwood and T. C. Gibb, *Mössbauer Spectroscopy*, Chapman and Hall, London, 1971.
44 C. S. Naiman, *J. Chem. Phys.*, 1961, **35**, 323.
45 (*a*) M. Duggan, N. Ray, B. Hathaway, G. Tomlinson, P. Brint and K. Pelin, *J. Chem. Soc., Dalton Trans.*, 1980, 1342; (*b*) R. J. Dudley, B. J. Hathaway, P. G. Hodgson, P. C. Power and D. J. Loose, *J. Chem. Soc., Dalton Trans.*, 1974, 1005.
46 B. J. Hathaway, in *Comprehensive Coordination Chemistry*, ed. G. Wilkinson, R. D. Gillard and J. A. McCleverty, Pergamon Press, Oxford, 1987, vol. 5, pp. 533–774.
47 (*a*) G. A. McLachlan, G. D. Fallon, R. L. Martin and L. Spiccia, *Inorg. Chem.*, 1995, **34**, 254; (*b*) S. J. Brudenell, L. Spiccia and E. R. T. Tiekink, *Inorg. Chem.*, 1996, **35**, 1974; (*c*) B. Graham, G. D. Fallon, M. T. W. Hearn, D. C. R. Hockless, G. Lazarev and L. Spiccia, *Inorg. Chem.*, 1997, **36**, 6366; (*d*) S. J. Brudenell, L. Spiccia, A. M. Bond, P. Comba and D. C. R. Hockless, *Inorg. Chem.*, 1998, **37**, 3705.
48 A. W. Addison, T. N. Rao, J. Reedijk, J. van Rijn and G. C. Verschoor, *J. Chem. Soc., Dalton Trans.*, 1984, 1349.
49 R. J. Parker, L. Spiccia, B. Moubaraki, K. S. Murray, B. W. Skelton and A. H. White, *Inorg. Chim. Acta*, 2000, **300–302**, 922.
50 (*a*) K. D. Karlin, J. C. Hayes, S. Juen, J. P. Hutchinson and J. Zubieta, *Inorg. Chem.*, 1982, **21**, 4106; (*b*) A. Nanthakumar, S. Fox, N. N. Murthy and K. D. Karlin, *J. Am. Chem. Soc.*, 1993, **115**, 8513; (*c*) R. R. Jacobson, Z. Tyeklar, J. Zubieta and K. D. Karlin, *Inorg. Chem.*, 1991, **30**, 2035; (*d*) N. Komeda, H. Nagao, G. Adachi, M. Suzuki, A. Uehara and K. Tanaka, *Chem. Lett.*, 1993, 1521.
51 G. P. Gupta, G. Lang, C. A. Koch, B. Wang, W. R. Scheidt and C. A. Reed, *Inorg. Chem.*, 1990, **29**, 4234.